



S.C. Breitzmann, S.Y. Lee

Department of Physics, Indiana University, IN 47405

K.Y. Ng

Fermilab, Batavia, IL 60510

(Dated: January 26, 2005)

Abstract

Passive ferrite inserts were used to compensate the space charge impedance in high intensity space charge dominated accelerators. We study the narrowband longitudinal impedance of these ferrite inserts. We find that the shunt impedance and the quality factor for ferrite inserts are inversely proportional to the imaginary part of the permeability of ferrite materials. We also provide a recipe for attaining a truly passive space charge impedance compensation and avoiding narrowband microwave instabilities.

PACS numbers: 52.59.Sa, 29.27.Bd, 29.20.-c

I. INTRODUCTION

High intensity high power hadron accelerators serve important functions for neutron sources and muon and neutrino factories. They also have industrial applications in power amplification and atomic transmutation. Particle beams in high intensity accelerators encounter large longitudinal and transverse space charge forces. The transverse space charge force can be alleviated by careful design of the accelerator lattice and a proper choice of betatron tune [1]. On the other hand, the longitudinal space charge force of the beam tends to spread out the bunch distribution to minimize the peak current. If longitudinal space charge is not properly controlled, the beam bunch can fill the beam gap, and this in turn leads to electron cloud instability for high intensity beams. At the Proton Storage Ring at Los Alamos National Laboratory, the rf cavity voltage must be increased in order to keep the beam bunched; this gives the electron cloud time to dissipate, and thus the instability is alleviated.

Since it is expensive to maintain a high rf cavity voltage, inductive inserts have been suggested to compensate the space charge impedance [2]. At the PSR, experiments with such inductive inserts have been performed [3]. With the inserts installed, the resulting longitudinal impedance becomes

$$\frac{Z_{\parallel}}{n} = -j \left[\frac{Z_0 g_0}{2\beta\gamma^2} - \omega_0 L \right], \quad (1)$$

where Z_0 is the vacuum impedance, g_0 is the geometry factor of the space charge impedance, and L is the effective inductance of the inductive inserts. In a coaxial transmission line approximation, the effective inductance is given by

$$L = \frac{\mu\ell}{2\pi} \ln \frac{b}{a}, \quad (2)$$

where a and b are the inner and outer radii of the inductive inserts, μ is the permeability of the ferrite material at low frequency, and ℓ is the total length of inductive inserts. In order to cancel the longitudinal space charge impedance, the length of the ferrite insert is

$$\ell = \frac{g_0 C}{2\beta^2\gamma^2\mu_r \ln(b/a)}, \quad (3)$$

where C is the circumference of the accelerator, and $\mu_r = \mu/\mu_0$ is the relative permeability of the ferrite at low frequency. Three ferrite inserts of a total length of 2.286 m were

added in order to cancel the space charge impedance. However, the installed inductive inserts themselves acted as another source of longitudinal instability peaked at the revolution harmonic 26 (72.67 MHz), and spontaneous self-bunching of the beam occurred [3, 4].

This spontaneous self-bunching has been carefully analyzed and found to have resulted from a narrowband impedance induced by these cavity-like ferrite inserts [5]. A solution to mitigate the narrow-band longitudinal microwave instability was proposed and successfully tested; by heating the ferrite, the permeability of the ferrite material is changed, and the narrowband impedance is detuned and broadened [6]. J.E. Griffin has carried out a TM_{010} standing wave model for the ferrite-lined cavity in order to provide analytic understanding of the narrowband impedance of these ferrite inserts [7]. Unfortunately, Griffin did not provide systematic study, and there was a deficiency in his formula that we will provide correction.

Although heating can change the properties of ferrite and provide a solution to mitigate the narrowband impedance, it is not the most desirable solution. It would be preferable to provide a truly passive device to counteract the space charge impedance. For this purpose, an analytic understanding of the narrowband impedance of these ferrite cavities would be helpful.

This paper offers a more systematic impedance calculation that can provide an understanding of the cavity impedance, which sometimes cannot easily be obtained by numerical programs in electromagnetism such as MAFIA. This paper is organized as follows: In Section II, we discuss the geometry of the ferrite insert and a model to calculate the impedance. We will compare our results with those obtained by MAFIA. The properties of impedance for the ferrite inserts are analyzed in Sec. III. Various applications of our model calculation are discussed in Section IV. The conclusion is addressed in Section V.

II. FERRITE INSERTS

For this analytical model and its resulting calculations, we follow the design of the ferrite modules installed in the PSR. A module consists of 30 ferrite rings with inner diameter 12.7 cm, outer diameter 20.3 cm, and thickness 2.54 cm. The ferrite cores line up end to end, so that one module looks like a hollow cylinder of ferrite without end faces. For this reason, the modules can be treated as rf cavities. In 1999 three modules were installed in the PSR, and the longitudinal microwave instability was observed to peak at 72.67 MHz or the $n = 26$

harmonic. Later it was found that heating the ferrite to a temperature of 125°C effectively alleviates this instability [5]. Two heated ferrite modules are routinely used in high intensity operation. We will carry out analytic calculation of the TM_{010} mode impedance for these ferrite cavities in this section.

A. Model

The ferrite ring is cylindrically symmetric, we thus use the cylindrical coordinate system. Since only the longitudinal particle motion concerns us, we consider only the fundamental TM_{010} mode, where the electric field is independent of the longitudinal coordinate s . In a uniform isotropic medium, the electromagnetic wave with $e^{j\omega t}$ obeys Maxwell's equation:

$$\frac{\partial^2 E_s}{\partial r^2} + \frac{1}{r} \frac{\partial E_s}{\partial r} + \frac{1}{r^2} \frac{\partial^2 E_s}{\partial \phi^2} + \frac{\partial^2 E_s}{\partial s^2} = -\omega^2 \mu \epsilon E_s$$

in both free space and the ferrite region. Here, μ and ϵ are permeability and permittivity of the uniform and isotropic medium.

We divide the ferrite cavity transversally into two regions. The first region, between $r = 0$ and $r = a$, consists of free space. (If we look at the module head on, a is the inner radius of the ferrite, and b is the outer radius of the ferrite, measured from the center of the core.) The second region is comprised of ferrite, and it occupies the space between $r = a$ and $r = b$. A cylindrical conducting beam pipe at $r = b$ encases the ferrite rings and is assumed to be a perfect conductor.

In vacuum, the wavenumber is $k = \omega \sqrt{\mu_0 \epsilon_0} = \frac{\omega}{c}$, and the electromagnetic fields are

$$\begin{aligned} E_s &= E_0 J_0(kr) \\ H_\phi &= j \frac{E_0}{\mu_0 c} J_1(kr). \end{aligned}$$

The longitudinal electric and azimuthal magnetic fields depend only on radial distance for the 010 mode.

In the ferrite region, the wavenumber k becomes

$$k_c = \omega \sqrt{\mu \epsilon} = k \sqrt{\epsilon_r (\mu' - j \mu'')}, \quad (4)$$

where ϵ_r is the relative permittivity and μ' and μ'' are the real and imaginary parts of the complex relative permeability, respectively. The intrinsic characteristic impedance of the

ferrite medium is

$$Z_c = \sqrt{\frac{\mu}{\epsilon}} = Z_0 \sqrt{\frac{\mu' - j\mu''}{\epsilon_r}}, \quad (5)$$

where $Z_0 = 377\Omega$ is the impedance of free space. The fields in the ferrite are then

$$\begin{aligned} E_s &= AH_0^{(1)}(k_cr) + BH_0^{(2)}(k_cr) \\ H_\phi &= \frac{j}{Z_c} [AH_1^{(1)}(k_cr) + BH_1^{(2)}(k_cr)], \end{aligned}$$

where $H_n^{(1)}$ and $H_n^{(2)}$ are Hankel functions with asymptotic waves e^{jk_cr} and e^{-jk_cr} respectively.

Specific boundary conditions must now be satisfied. Namely, at $r = b$ the longitudinal electric field must be zero due to the presence of the assumed perfectly conducting cavity wall. In addition, the longitudinal electric fields and azimuthal magnetic fields must be matched from one medium to the other. Thus

$$AH_0^{(1)}(k_cb) + BH_0^{(2)}(k_cb) = 0 \quad (6)$$

$$E_s(a^-) = E_s(a^+), \quad (7)$$

$$H_\phi(a^-) = H_\phi(a^+). \quad (8)$$

There are now three equations, and there are three unknowns: A , B , and k_c . Solving Eq. (6) for B in terms of A and entering the result into Eq. (7) gives

$$A = E_0 \frac{J_0(ka)H_0^{(2)}(k_cb)}{H_0^{(1)}(k_ca)H_0^{(2)}(k_cb) - H_0^{(1)}(k_cb)H_0^{(2)}(k_ca)} \quad (9)$$

If instead one inserts B (in terms of A) into Eq. (8), one finds

$$A = \frac{Z_c}{Z_0} E_0 \frac{J_1(ka)H_0^{(2)}(k_cb)}{H_1^{(1)}(k_ca)H_0^{(2)}(k_cb) - H_0^{(1)}(k_cb)H_1^{(2)}(k_ca)} \quad (10)$$

The resonance condition can be obtained by equating Eqs. (9) and (10).

To calculate the longitudinal impedance, the general formula is $\Delta V = -IZ_{\parallel} = -E_s\ell$, where E_s is the longitudinal electric field and ℓ is the total length. Using Ampere's law, $I = \oint Hdl = 2\pi aH_\phi$, we obtain

$$\begin{aligned} \frac{Z_{\parallel}}{\ell} &= -\frac{E_s}{2\pi aH_\phi} = -\frac{\mu_0 c J_0(ka)}{2\pi a j J_1(ka)} \\ &= j \frac{Z_c}{2\pi a} \frac{H_0^{(1)}(k_ca)H_0^{(2)}(k_cb) - H_0^{(1)}(k_cb)H_0^{(2)}(k_ca)}{H_1^{(1)}(k_ca)H_0^{(2)}(k_cb) - H_0^{(1)}(k_cb)H_1^{(2)}(k_ca)}. \end{aligned} \quad (11)$$

Here the relation between $J_0(ka)$ and $J_1(ka)$ is obtained by the continuity conditions. This formula gives the impedance per unit length on the axis of the cavity as a function of frequency, which is embedded in the k_c .

In general, the permeability of all ferrite materials is a complicated function of frequency. Figure 1 shows the “derived” relative permeability as a function of frequency for Ni-Zn ferrite cores M4C21A [5]. C. Beltran has obtained these values of the complex permeability by fitting the measured S_{11} parameter of the two-port network driven by source frequencies spanning 0 to 120 MHz [5]. The effective impedance at a given frequency is obtained by Eq. (11) with the permeability of that frequency. Since the complex permeability is measured and analyzed at a discrete number of frequencies, we approximate the intermediate frequencies by linear interpolation as shown in Fig. 1.

B. Results and Comparisons

First we consider the ferrite core dimensions and length for three modules, and calculate the impedance at each frequency for which the value of μ is known and $\epsilon_r = 15$ from the manufacturer’s data sheet. Figure 2 compares the impedance per unit length and per unit harmonic of our model and those obtained by the MAFIA code [5]. The real and imaginary curves from the model and from C. Beltran agree quite well in shape and peak location but differ slightly in magnitude. Overall there is good agreement.

III. PROPERTIES OF THE IMPEDANCE FOR THE FERRITE INSERT

Since our model calculation agrees well with the numerical calculation of MAFIA, we can study general properties of the ferrite inserts. With the definition of the Hankel function, the impedance in Eq. (10) can be expressed as

$$\frac{Z_{\parallel}}{\ell} = j \frac{Z_c}{2\pi a} \frac{J_0(k_c b)Y_0(k_c a) - J_0(k_c a)Y_0(k_c b)}{J_0(k_c b)Y_1(k_c a) - J_1(k_c a)Y_0(k_c b)}, \quad (12)$$

where $J_n(z)$ and $Y_n(z)$ are Bessel and Neumann functions. The relative permittivity of the ferrite is fixed at $\epsilon_r = 15$, and the permeability is shown in Fig. 1.

A. Low frequency limit

At low frequency, $k_c a$ and $k_c b$ are both small numbers, so we use the small argument expansion for Bessel and Neumann functions to obtain

$$\frac{Z_{\parallel}}{\ell} \approx j \left(\frac{\omega \mu}{2\pi} \ln \frac{b}{a} \right) \left(\frac{J_0(k_c a) J_0(k_c b) + 1.5 k_c^2 (b^2 - a^2) / (8 \ln b/a)}{1 - \frac{1}{4} (k_c b)^2 + \frac{1}{2} (k_c a)^2 \ln(b/a)} \right). \quad (13)$$

The first factor in Eq. (13) corresponds to the inductive impedance of coaxial line as shown in Eq. (2), while the second factor is the geometric factor. Figure 3 compares the impedances obtained from numerical calculations and the coaxial approximation with $\mu' = 38$ at $\omega \rightarrow 0$ at 25°C (see Fig. 1). These calculations were carried out with a fixed inner radius of $a = 6.0$ cm and varying outer radii from $b = 8.0$ cm to 17.0 cm in step of 0.5 cm.

B. Resonance

The impedance in Eq. (12) has a maximum at a resonance condition given by the zeros of the denominator:

$$J_0(k_{c,r} b) Y_1(k_{c,r} a) - J_1(k_{c,r} a) Y_0(k_{c,r} b) = 0, \quad (14)$$

where $k_c = (\omega/c) \sqrt{\epsilon_r (\mu' - j\mu'')}$. Figure 4 shows the impedances for the outer radii $b = 10$ cm, 11 cm, 12 cm, and 12.5 cm respectively. We note that as the outer radius increases, the resonance frequency is shifted lower, and the peak of impedance becomes much larger.

To understand the resonance of the impedance, we examine the behavior of the denominator, Eq. (14) as a function of frequency. Figure 5 shows the real (circle) and the imaginary (crosses) parts of the impedance for $b = 10$ cm (bottom plot) and $b = 12$ cm (top plot) cases. The real (solid) and the imaginary (dash-dots) parts of Eq. (14), and the real (dashes) and imaginary (dots) parts of the numerator of Eq. (12) are also shown in Fig. 5. Note that the peak in the impedance corresponds to the zero of the real part of the denominator. Although one can calculate the values of the denominator as a function of frequency, there is no analytic formula to describe the zero of Eq. (14). However, the resonance location can be well described by $|k_c|(b-a) \approx 2.0$ in the region where μ'' is small, as shown in the lower plot of Fig. 6.

Near the resonance frequency, the magnitude of the numerator is nearly constant, while the real part of the denominator vanishes at the resonance. The resulting impedance can be

fitted by an RLC-circuit model:

$$\frac{Z}{n\ell} = \frac{\omega_0}{\omega} \frac{R_{\text{sh}}}{1 + jQ(\omega/\omega_r - \omega_r/\omega)}. \quad (15)$$

The upper plot of Fig. 6 shows the fitted parameters R_{sh} (in $\text{k}\Omega/\text{m}$), Q , and f_r (in MHz) as a function of the outer radii b from 8.0 cm to 16.0 cm. In particular, we find the geometric factor R_{sh}/Q is nearly constant.

Both the shunt impedance R_{sh} and the quality factor Q depend on the imaginary part of the permeability. Figure 7 plots the R_{sh} and Q vs the μ'' . Both R_{sh} and Q are inversely proportional to the imaginary part of the permeability.

IV. APPLICATIONS

The passive inductive insert concept is a very useful method to combat the large space charge impedance for high intensity low energy accelerators. Since the actual experiment indicates that the narrowband impedance can induce microwave instability and cause beam loss, it becomes important to find a possible solution to de-Q these inductive inserts.

A. Heating Ferrite

Currently the ferrite inserts in the Proton Storage Ring must be heated to mitigate the narrowband impedance that leads to spontaneous self-bunching. Based on Fig. 1, we observe that the heating of ferrite produces two major effects: (1) μ' increases from 38 to 60 at low frequency, and (2) μ'' increases from 14.5 to 34 at the resonance frequency of $f = 75$ MHz. The first effect provides space charge compensation with a much shorter length of ferrite cavities. Thus two heated ferrite inserts can provide more inductive compensation than three ferrite inserts operating at the room temperature. The second effect shows that both the shunt impedance R_{sh} and the quality factor Q are reduced by a factor of 0.40. Thus two ferrite cavities with the same geometry can mitigate the microwave instability, and provide space charge compensation.

However, it is a nuisance to heat the ferrite in an accelerator environment. It is more desirable to design a completely passive system whenever possible. To this end, the model presented here may be used to find a better cavity geometry whose unheated impedance is similar to that of the present (heated) inserts.

B. Mitigation of microwave instability with geometric variation

We note that the ferrite cavities installed in the PSR have an impedance of about $R_{sh} \approx 6.5 \text{ k}\Omega$ and $Q \approx 3.5$. To de-Q these cavities, we can install cavities with different geometry. We note that the cavities with outer radii b larger than 11 cm have Q values much too large for compensation. Furthermore, the resonance frequency for b larger than 11 cm does not vary as much and thus does not de-Q as easily. The most beneficial solution is to install cavities with 10 cm, 9.5 cm and 9.0 cm outer radii.

To avoid microwave instability induced by a narrowband resonance, the stability threshold of the UV diagram is a useful indicator, where one defines

$$U' + jV' = \frac{eI_0(Z_{||}/n)}{\beta^2 E \delta_{FWHM}^2 |\eta|} = \Gamma \frac{Z_{||}}{n}. \quad (16)$$

Using the parameters of PSR: beam energy $E = 1.736 \text{ GeV}$ ($\beta = 0.84$), the peak current $I_0 = 74 \text{ A}$ for $9.0 \text{ }\mu\text{C}$ circulating charge with 290 ns bunch length, $V_{rf} = 14 \text{ kV}$, the phase slip factor of $|\eta| = 0.185$, the FWHM beam momentum spread for a Gaussian beam of $\delta_{FWHM} = \sqrt{8 \ln 2} \sigma_\delta$ with $\sigma_\delta = 2.66 \times 10^{-3}$, we obtain $\Gamma = 8.35 \times 10^{-3}$. Assuming the geometry factor $g_0 = 3$, the space charge impedance is $Z_{sc} = -j196 \text{ }\Omega$. Figure 8 plots V' vs. U' parameters for (1) the impedance of the ferrite cores installed in the PSR (circles and crosses symbols), (2) a 2m long (3:2:1) combination of 9.0 cm, 9.5 cm, and 10.0 cm OD ferrite inserts (the blue solid line), (3) a 2m long (5:1) combination of 9.0 cm and 10.0 cm OD ferrite inserts (the dotted line), (4) stability threshold (solid line), and (5) unstable line (red dashed line) with a growth rate of 0.4 ms. Points that fall inside the stability curve will be stable, while points that fall outside the curve will be unstable. We note that the impedance of the heated ferrite inserts is below the microwave instability threshold, while the impedance of the room temperature ferrite inserts is far above the threshold. We also note that the combination of ferrite inserts is able to detune the cavity Q-value so that the final impedance is within the stability threshold.

V. CONCLUSION AND DISCUSSIONS

We found that the analytic TM_{010} model of the cylindrical symmetric ferrite insert provides a good description of the narrowband impedance and agrees well with work previously done using MAFIA. With this analytic model, we have conducted a systematic study of the

properties of ferrite inserts with different geometries. We find that the shunt impedance and the quality factor of the TM_{010} mode are inversely proportional to the imaginary part of the permeability. We also find that the resonance condition is approximately given by $|k_c|(b-a) \approx 2$, where $k_c = (\omega/c)\sqrt{\epsilon_r(\mu' - j\mu'')}$. In fact, these properties can be used to determine the permeability of ferrite materials by carrying out impedance measurements of ferrite cores.

With the results presented here, we find that passive space charge compensation is possible by properly chosen ferrite inserts with various geometries without inducing microwave instability. Careful calculation before implementing the space charge compensation would be important in minimizing agonizing side effects of passive compensation encountered in the PSR. It is indeed possible to produce fixed ferrite inserts, and install them in a high intensity low energy ring for passive space charge compensation.

Acknowledgments

This work is supported in part by grants from the US Department of Energy: US DOE DE-FG0292ER40747, and NSF PHY-0244793.

-
- [1] See e.g. S. Cousineau, Ph.D. Thesis, Indiana University (2002); and references therein.
 - [2] V.K. Neil and R.J. Briggs, *Plasma Phys.* **9**, 631 (1967); R.J. Briggs and V.K. Neil, *J. Nucl. Energy, Part C* **8**, 255 (1966).
 - [3] M.A. Plum et al, *PRST-AB*, **2**, 064201 (1999).
 - [4] R. Macek, private communications
 - [5] C. Beltran, Ph.D. thesis, Indiana University (2003).
 - [6] M. Popovic, private communication.
 - [7] J.E. Griffin, "Radial Transmission Line Treatment of Spurious Resonance in Ferrite Cylinder Space Charge Compensation System." (unpublished)

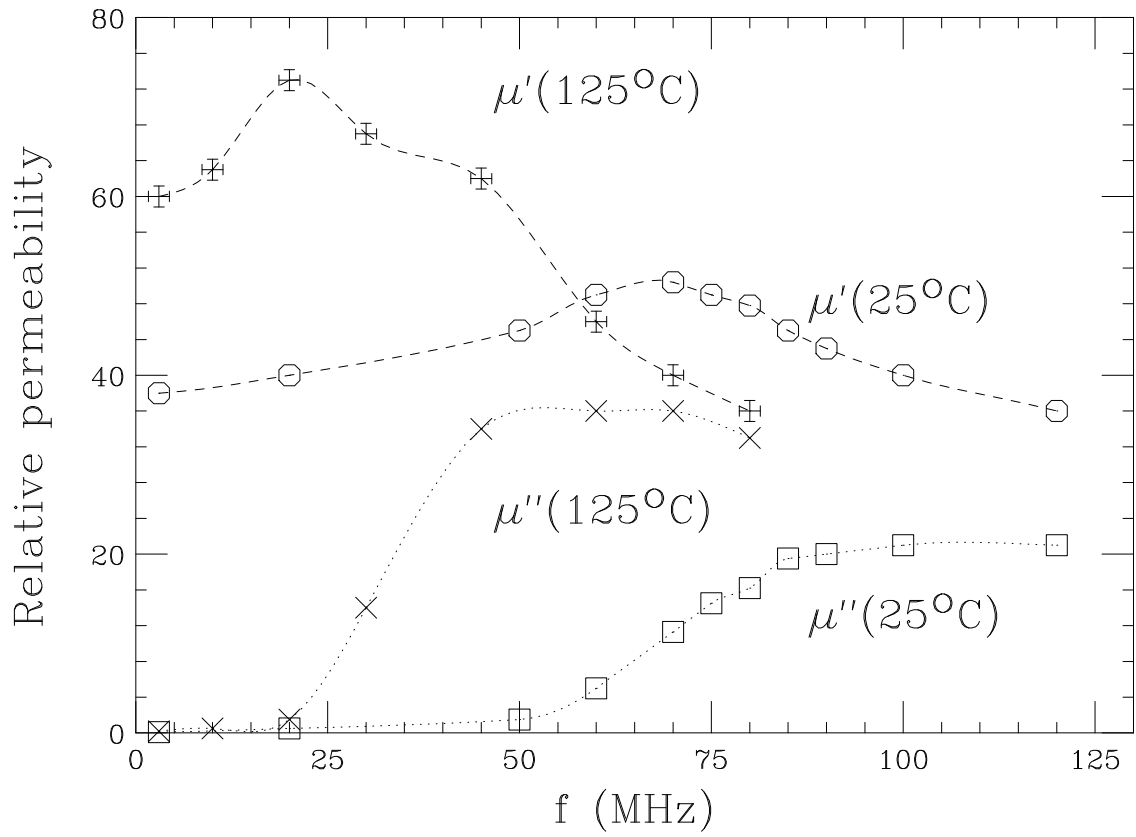


FIG. 1: Real and imaginary parts of the complex permeability at different frequencies (From Chris Beltran [5].)

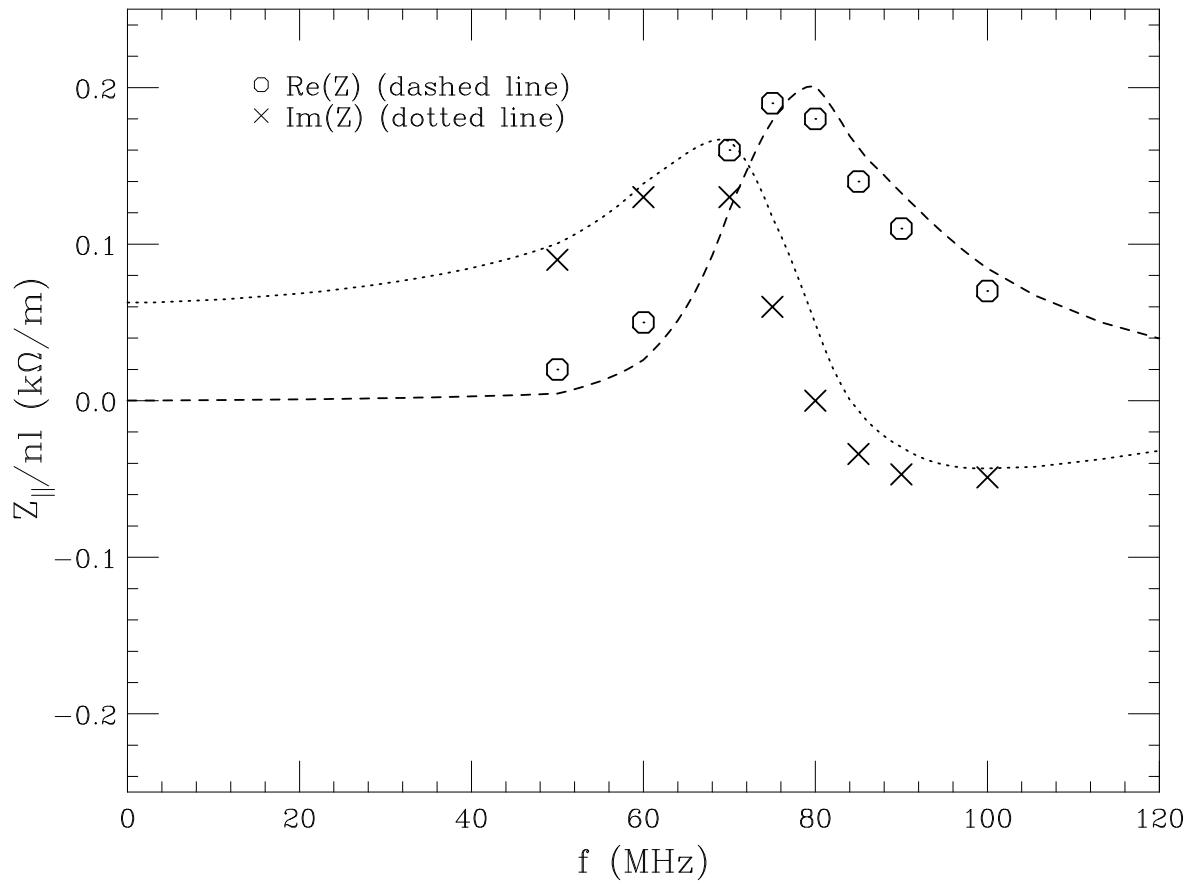


FIG. 2: Comparison of real and imaginary impedances from the model and Chris Beltran's MAFIA calculations shown as circles and X'es. In this calculation, the ferrite ring parameters are $a = 6.35$ cm, $b = 10.15$ cm, at room temperature of 25°C .

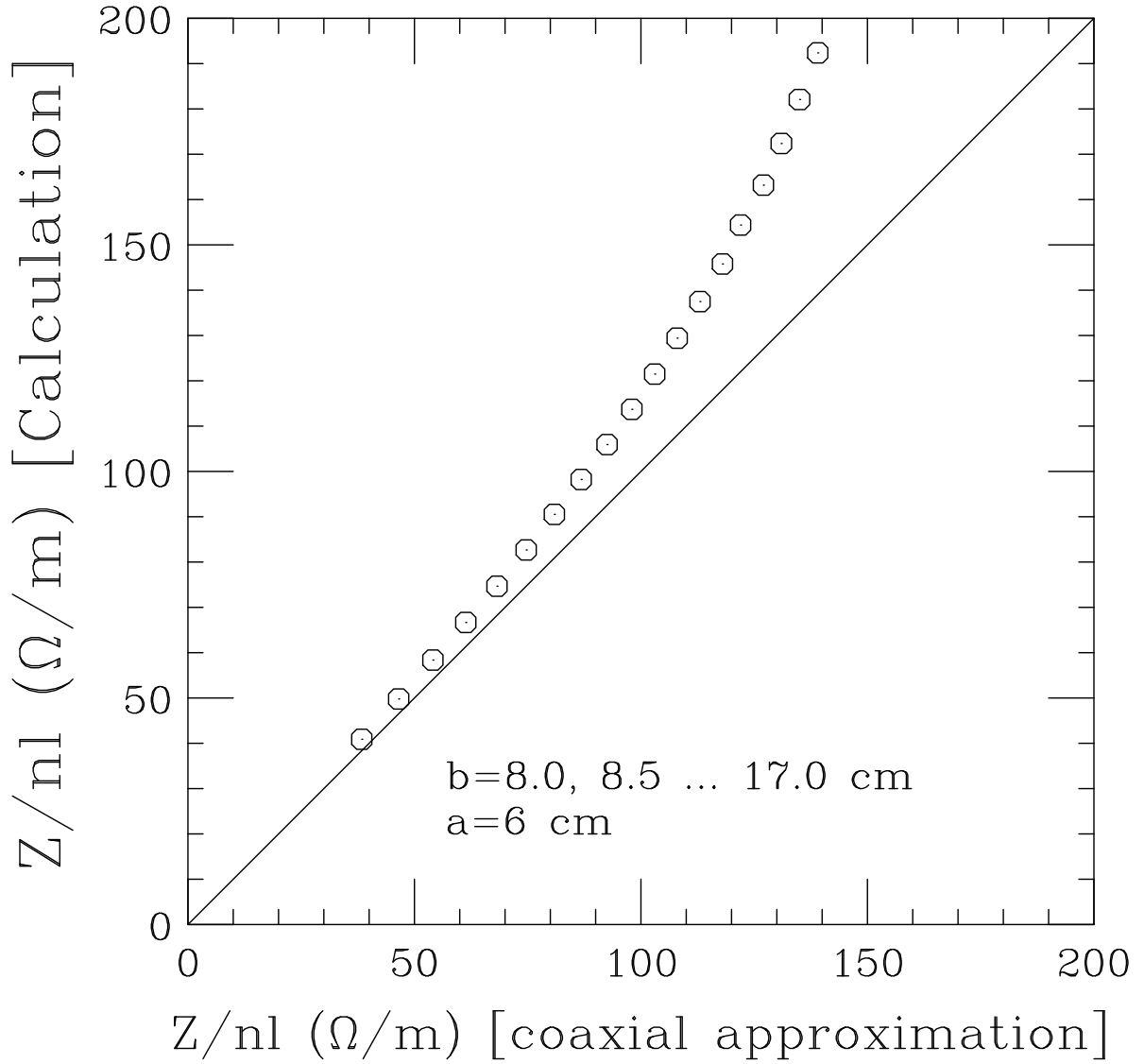


FIG. 3: The imaginary part of the impedance divided by the mode number n at low frequency is compared with the theoretical coaxial approximation of Eq. (1) for a fixed inner radius $a = 6$ cm and varying outer radii from $b = 8.0$ cm, 8.5 cm, \dots , 17.0 cm. The horizontal axis is proportional to $\ln(b/a)$. Note that the coaxial approximation is very good when the ratio of b/a is not large. The geometric factor becomes larger than 1 if the ratio of $b/a > 1.5$.

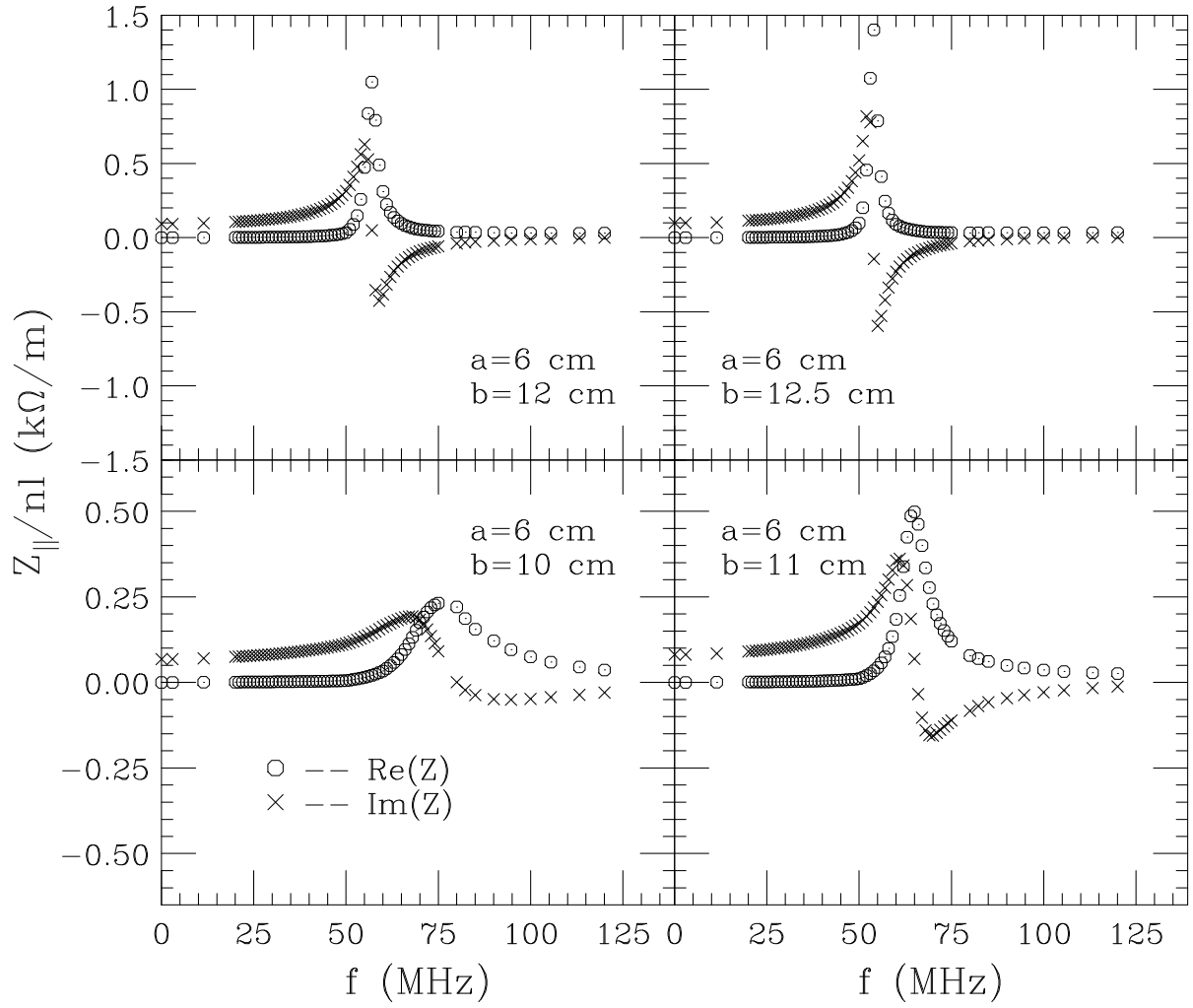


FIG. 4: Impedance per unit length per harmonic is calculated for ferrite cores with inner radius 6 cm and outer radii 10, 11, 12, and 12.5 cm. Note that the peak frequency is lowered, and the magnitude of the impedance becomes larger as the outer radius of the ferrite core increases.

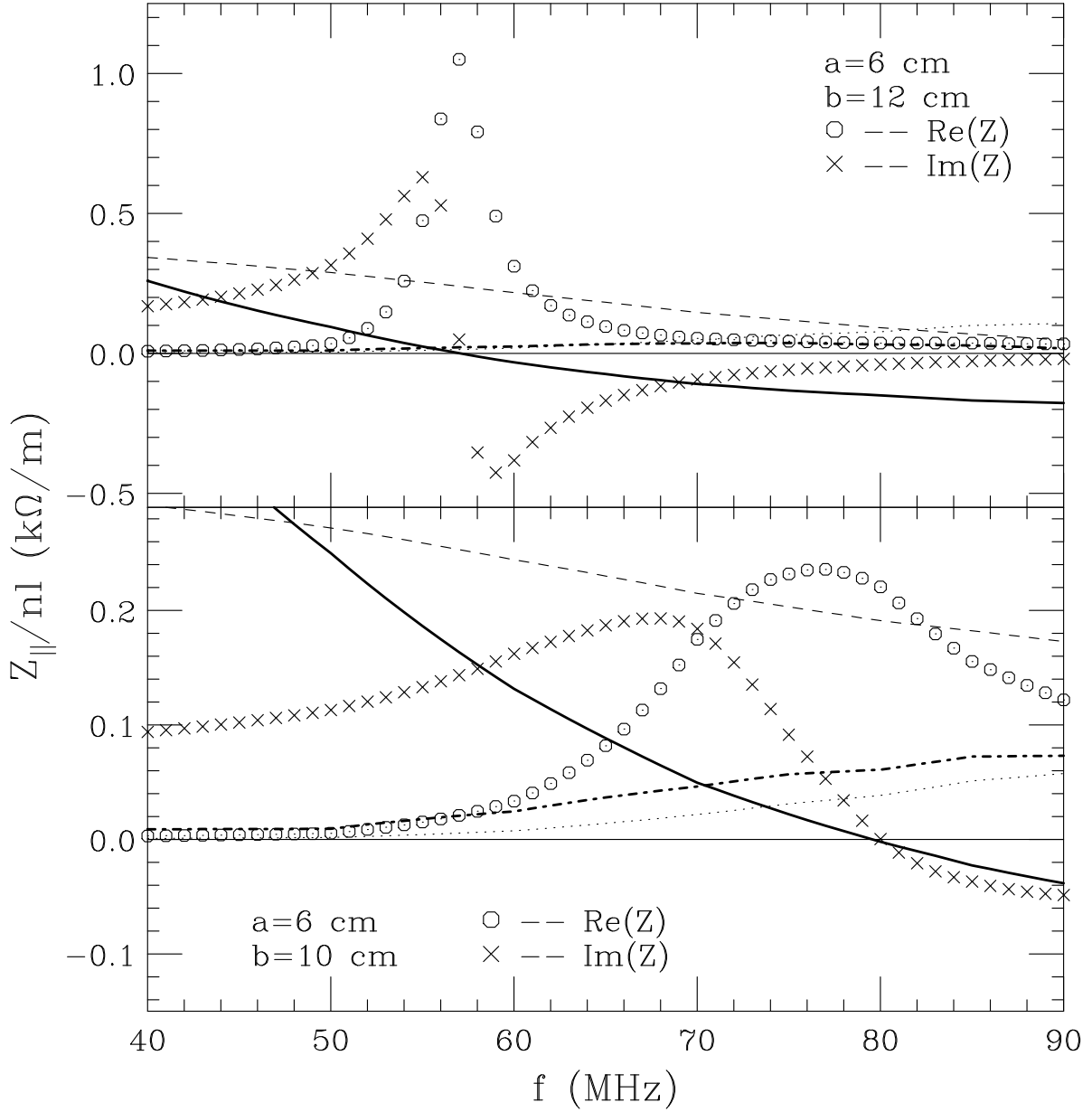


FIG. 5: The real (circle symbol) and imaginary (cross symbol) parts of impedance divided by the mode number n for $a = 6$ cm, $b = 10$ cm (bottom) and $b = 12$ cm (top). The real and imaginary parts of the numerator $J_0(k_c b)Y_0(k_c a) - J_0(k_c a)Y_0(k_c b)$ are plotted as a function of frequency f in dashed and dotted lines. The real and imaginary parts of the denominator $J_0(k_c b)Y_1(k_c a) - J_1(k_c a)Y_0(k_c b)$ are plotted as a function of frequency f in solid and dash-dotted lines respectively. Note that the vanishing real part of the denominator corresponds to the peak of the narrowband TM_{010} mode.

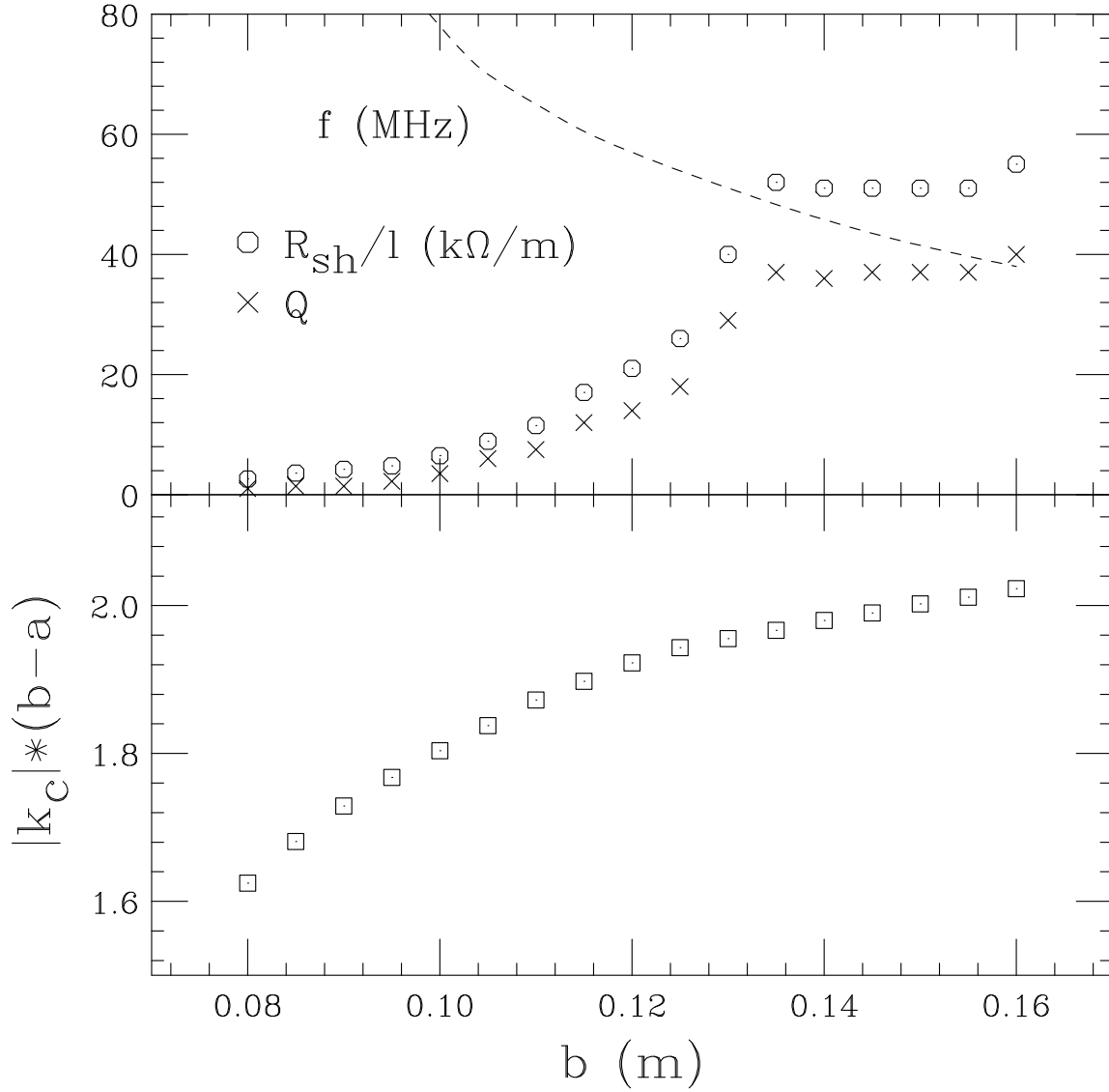


FIG. 6: The RLC circuit parameters that fit the impedance are plotted in this figure. Upper plot: the resonance frequency f_r in MHz (dash line), the shunt impedance in (kΩ/m), and the quality factor Q are plotted as function of the outer radius b . Lower plot: The resonance wave number $k_c \cdot (b - a)$ is plotted as a function of the outer radius b . Here the resonance wave number is $k_c = (\omega_r/c)\sqrt{\epsilon_r(\mu' - j\mu'')}$. Note that $|k_c| \cdot (b - a) \approx 2.0$ seems to describe the zero of the denominator and the peak of the impedance of the TM_{010} mode.

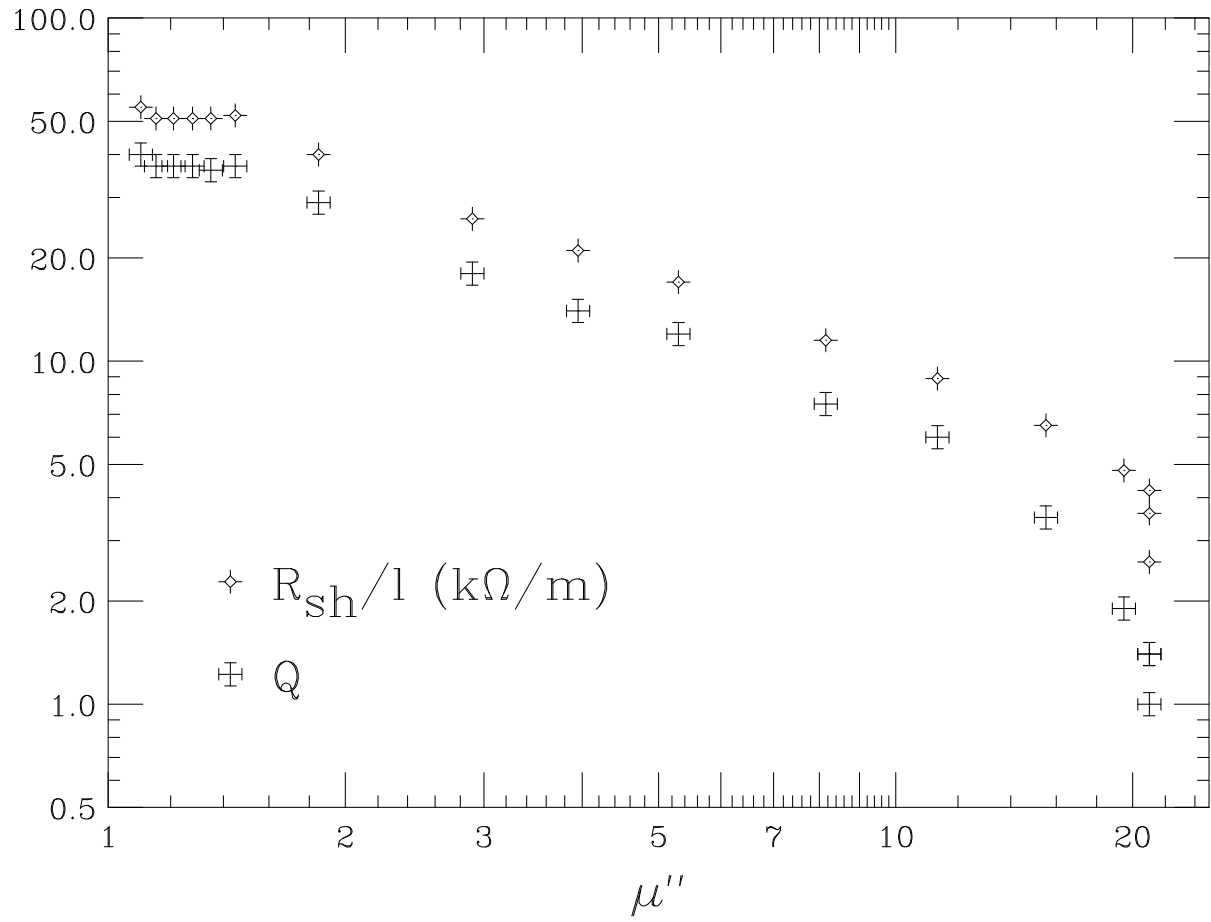


FIG. 7: The shunt impedance R_{sh} and the quality factor Q derived from fitting the impedance with RLC-circuit model are plotted as a function of μ'' . Note that both R_{sh} and Q are inversely proportional to the imaginary part of the permeability μ'' .

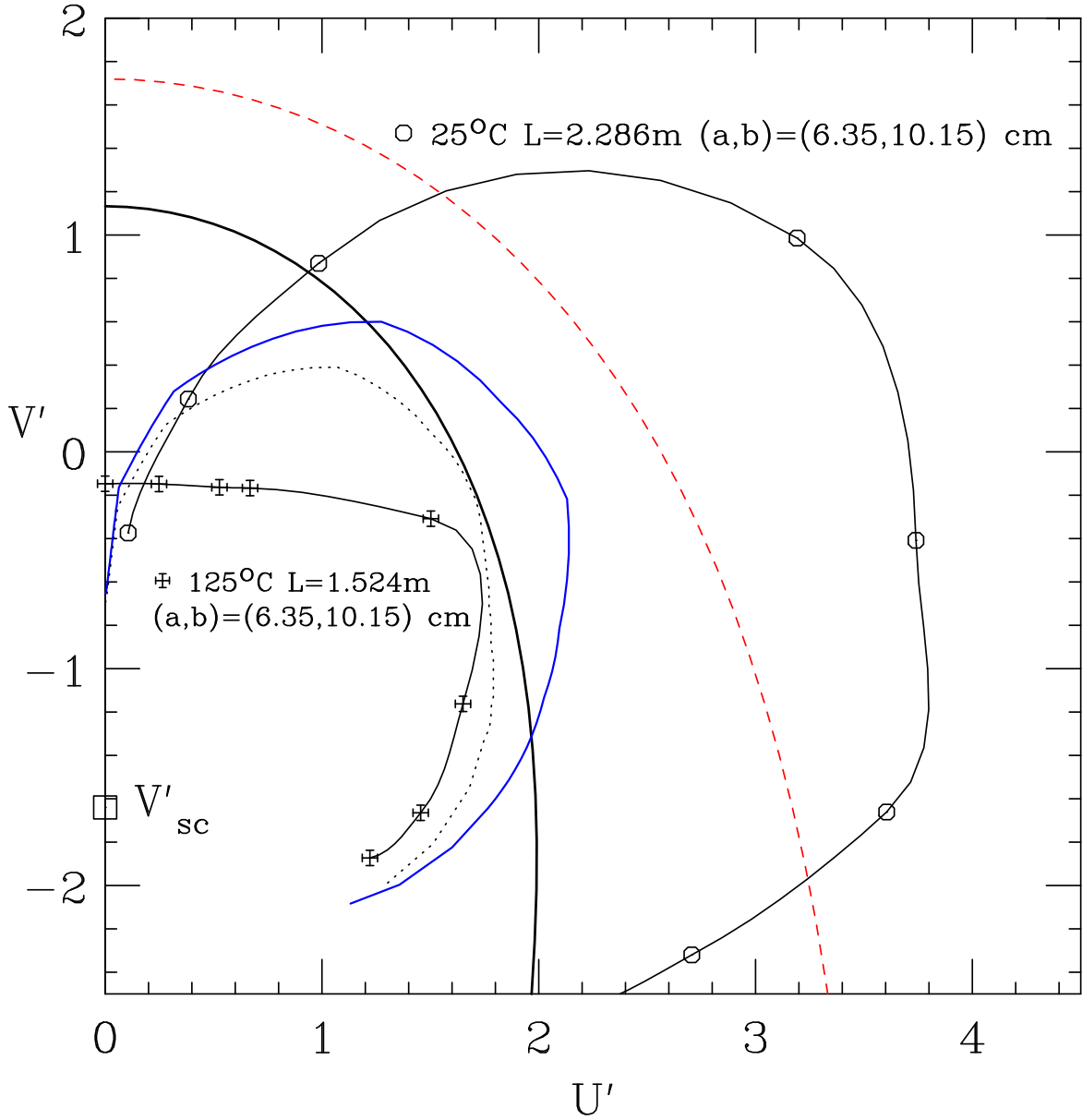


FIG. 8: Stability comparison of different core thickness for a Gaussian beam. The U' and V' parameters for the 3 room-temperature ferrite inserts (2.286 m) are plotted as circle symbol. The U' and V' of the 2 heated ferrite-inserts (1.524 m) are plotted as cross symbol. The dotted line corresponds to a 2.0 m ferrite insert of $b = 9.0$ cm and 10 cm in 5:1 ratio. The blue solid line corresponds to a de-Qed 3:2:1 combination of 9.0 cm, 9.5 cm, and 10 cm core inserts of a total length of 2.0 m. The red dashed line corresponds to an instability growth rate of 0.4 ms. Beam parameters of this calculation are listed in the text.